©1983 Geologie en Mijnbouw 0016-7746/83/6203-0499 $ 2.50/0

MEGARIPPLE CROSS-BEDDING AS A TOOL FOR THE RECONSTRUCTION OF THE PALAEO-HYDRAULICS IN A HOLOCENE SUBTIDAL ENVIRONMENT, S.W. NETHERLANDS[1]

S.D. NIO[2], C. SIEGENTHALER[3] & C.S. YANG[4]

ABSTRACT

Nio, S. D., C. Siegenthaler & C. S. Yang 1983 Megaripple cross-bedding as a tool for the reconstruction of the palaeo-hydraulics in a Holocene subtidal environment, S.W. Netherlands. In: M. W. van den Berg & R. Felix (eds.): Special issue in the honour of J.D. de Jong – Geol. Mijnbouw 62: 499-510.

Large-scale cross-bedded sets from a Holocene subtidal sequence exposed in a construction pit at the mouth of the Oosterschelde were used for comparative studies with present-day tidal processes. The periodic variation which can be observed within a large-scale cross-bedded set of a subtidal megaripple is used to reconstruct the tidal hydraulic parameters such as the shear velocity, the tidal current velocity and the tidal range. In addition to this, the aperiodical variation of the set is used to evaluate the storm-induced components of these parameters. The main steps of the procedure are: (1) the identification of the tidal features of the set such as the lateral bundle sequence; (2) an appropriate selection of the sediment transport rate function; and (3) the development of a function relating the tidal range with the shear velocity based on an estimate of the water depth. Additionally a simple expression is derived, which relates the ratio of the astronomical tides and the atmospheric disturbance to the mean standard deviation of the bundle thicknesses. The calculated tidal current velocities, tidal ranges and its standard deviations from a subrecent example show a good agreement with the actual hydraulic parameters.

INTRODUCTION

A large part of the Holocene is presently exposed in a construction pit at the mouth of the Oosterschelde tidal basin, SW Netherlands (Fig. 1). The Holocene sequence can be observed down to a depth of 15 m below mean sea-level. The lower part consists of cosets of large-scale cross-bedded units (Fig. 2), which consist of fine sand with a mean diameter of 0.02 cm. Palaeogeographic reconstructions from old maps and the occurrence of *Mya arenaria* in the deposits, which was imported from the Atlantic coast of North America at the end of the 16th Century, indicate the presence of a relatively large tidal channel during the 17th and the 18th century (VAN DEN BERG, 1982); the exposed sequence is interpreted as part of the aggradational tidal channel complex (VISSER, 1980; VAN DEN BERG, 1981, 1982). Measurements show that the megaripple foresets dip towards the N and the NW, indicating that the ebb current was the dominant process in the creation of the lower sequence.

Comparative studies with the present-day analogues showed that this and other tidal channel complexes in the area were very dynamic (VAN DEN BERG, 1982). Fast lateral migration, caused by erosion along the outer margins of channels and considerable acretion along the inner margins, characterized its sedimentation pattern. These conditions bring about a high preservation potential of the different bedforms. Features produced by the semi-diurnal tidal cyclicity as well as neap-spring tidal periods were well preserved within the sequence of the large-scale cosets, described as the lateral bundle sequence (VISSER, 1980).

In the lateral bundle sequence, the foresets are separated at more or less regular intervals by thin mud drapes and/or erosional reactivation surfaces (Fig. 3). Each foreset unit bounded by these mud drapes or reactivation surfaces is defined as a bundle (BOERSMA, 1967, 1969; VISSER, 1980). VISSER (1980) and later ALLEN (1981a) proved that each bundle was formed during a single dominant tide and that the mud

[1] Manuscript received: 1983-02-17.
Manuscript accepted: 1983-03-16.
Comparative Sedimentology Division, Publication nr. 30.

[2] Comparative Sedimentology Division, University of Utrecht, The Netherlands.
[3] Federal Institute of Technology, Geological Institute, Zürich, Switzerland.
[4] Ministry of Geology and Minerals, Bureau of Marine Geology Survey, Shanghai, China, present address ([2]).

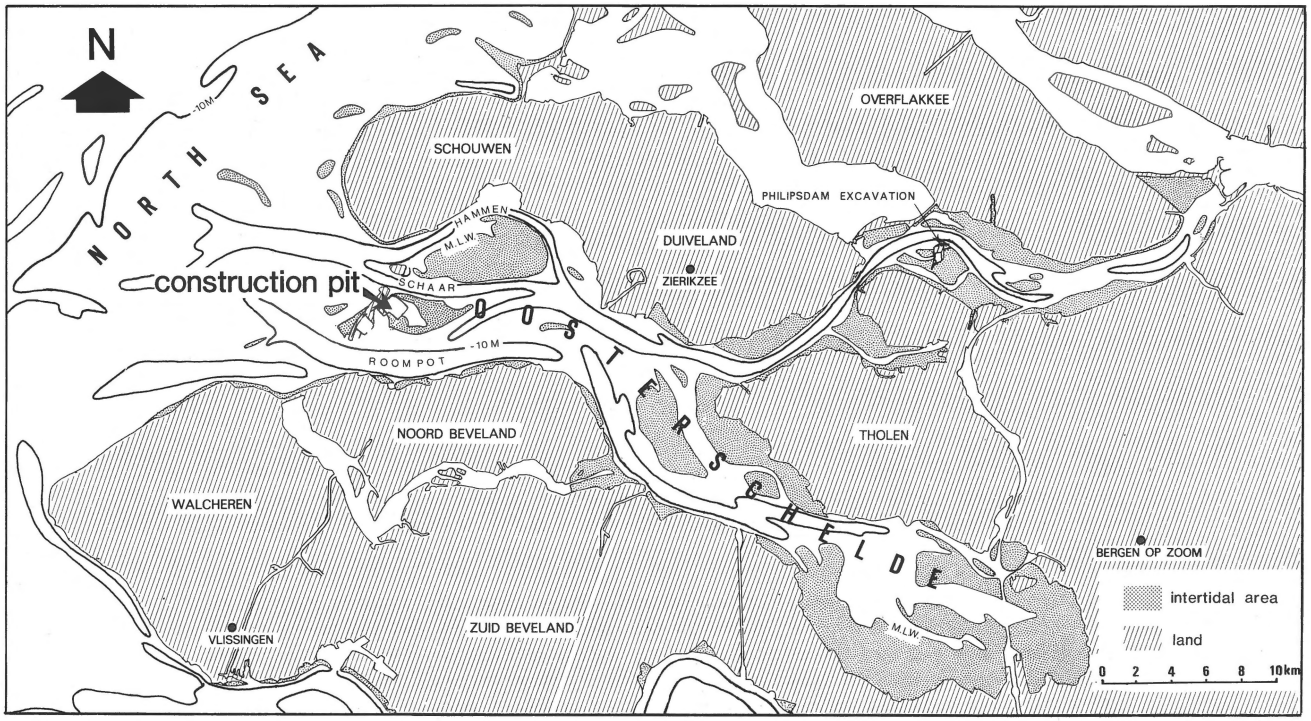

Fig. 1
Physiographic map of the Oosterschelde basin with location of the construction pit.

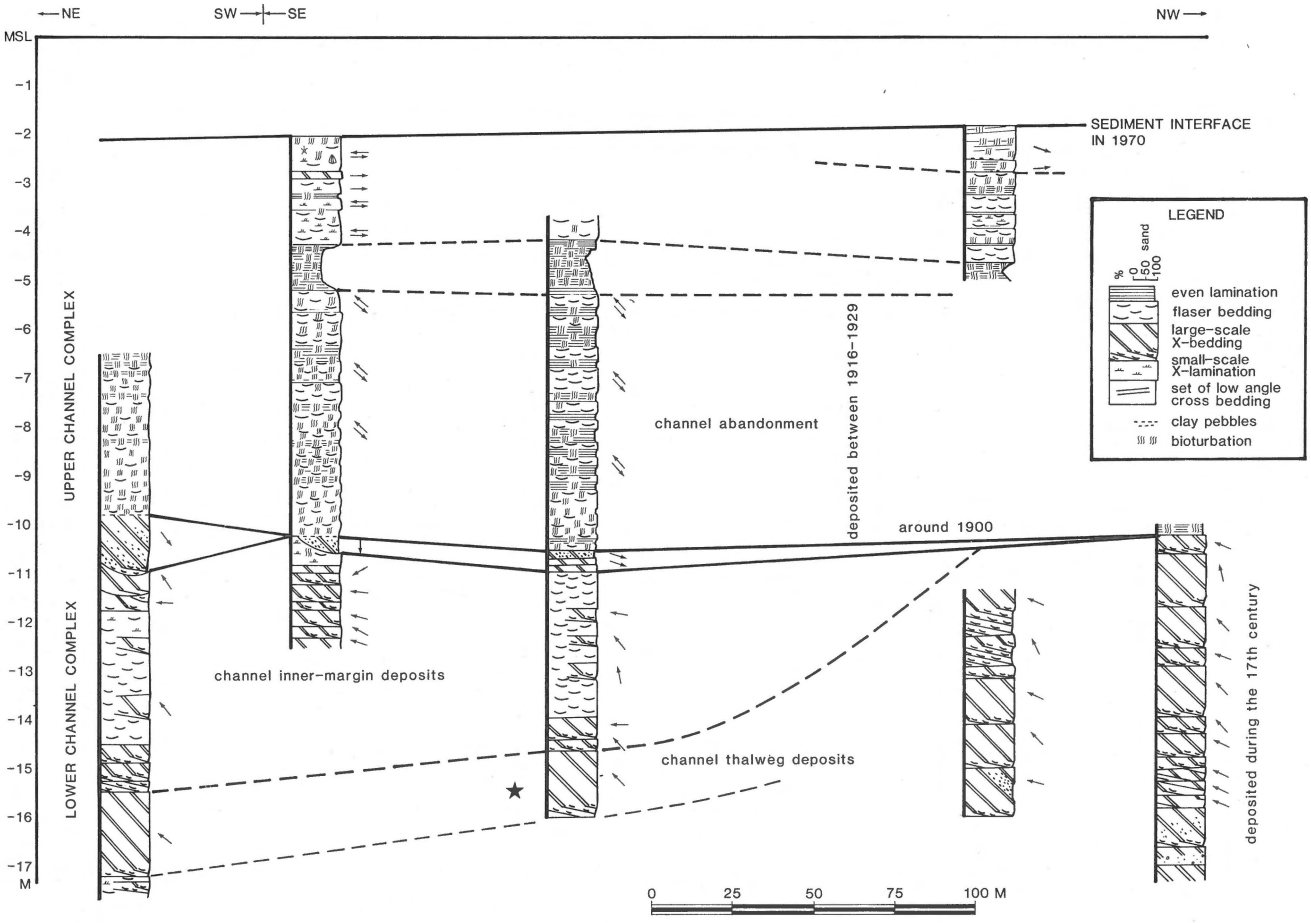

drapes below and above the bundle were formed during the slackwater periods after respectively the subordinate and dominant tidal current phase. The terms dominant and subordinate refer to asymmetrical bidirectional tidal currents where the tidal currents in one direction are stronger as compared to those in the opposite direction.

Because of the unique relationship between tidal processes and its preserved cyclic succession or lateral bundle sequence observed in the Oosterschelde, there is a good chance of calculating palaeo-hydraulic parameters from ancient subtidal deposits. ALLEN (1981b) suggested a method to calculate palaeotidal speeds and the relative ratio between neap and spring tidal ranges based on examples from the Cretaceous Folkstone Beds in England and the Holocene deposits of the Oosterschelde mouth. ALLEN & HOMEWOOD (in press) more recently estimated the palaeohydraulics of the Miocene sand waves in Swiss molasse using the parameters of the critical shear velocities for the ripple-dune transition and the dune-plane bed transition.

Some major problems in this quantitative evaluation of clastic tidal deposits remain unsolved. The crucial points which will be discussed in this paper are:

1. The selection of an appropriate bed-load transport function.
2. The approximation of the time-dependent pattern of the tidal currents and the estimation of the integration of this pattern over the dominant tidal half cycle. ALLEN (1981b) used this integration for his calculations. This method, however, proved to be complicated and difficult (see also LANGHORNE, 1981). TEYSSEN (in press) modified this method. However, many problems remain unsolved. An additional problem in ancient clastic tidal deposits is the unknown time dependent pattern of tidal currents. To solve this problem, a different approach is applied in this paper.
3. The development of a function, which relates the tidal range with the shear velocity based on an estimated water depth.
4. The derivation of a simple expression which relates the ratio of the astronomical tides and the atmospheric disturbance to the mean standard deviation of the bundle thicknesses.

THE RELATIONSHIP BETWEEN THE LATERAL BUNDLE SEQUENCE AND TIDAL HYDRAULICS

VISSER (1980) and ALLEN (1981a) described large-scale cross-bedded sets with lateral bundle sequences deposited in subtidal environments. The characteristic features of the lateral bundle sequence can be summarized as follows:

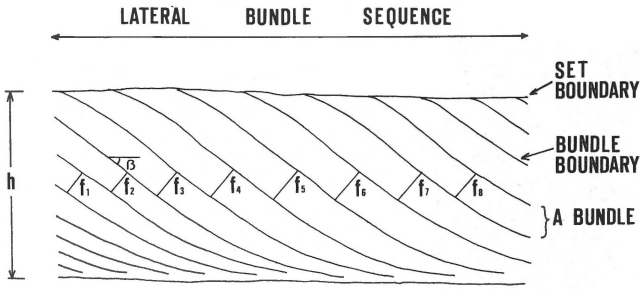

Fig. 3
Schematic drawing of the lateral bundle sequence and its geometry. The bundle boundaries are characterized by thin mud drapes and/or erosional reactivation surfaces. β: the dip of the foreset plane. f_1, ..., f_8: the thicknesses of successive bundles, measured perpendicular to bundle boundary. h: the set height as an estimate of the original megaripple height.

- The characteristic bundle boundaries defined by:
  (1) thin mud drapes, deposited during the slackwater periods, and thin sandy layer between the mud drapes, deposited by the subordinate currents. These features often produce the so-called mud drape couplets (VISSER, 1980).
  (2) erosional reactivation surface between two tidal bundles, indicating erosion of the mud drape by the subordinate current.
  Each bundle with its characteristic boundaries reflects a complete ebb-flood tidal cycle.
- The pattern of lateral thickening and thinning of the bundles reflects the neap-spring tide periods as well as the daily inequality (VISSER, 1980; ALLEN, 1981a; VISSER & DE BOER, in press).
- An aperiodic random thickness variation component caused by storms, which shows a tendency for a negative thickness auto-correlation of successive bundles, i.e. thick bundles tend to be compensated for by subsequent thin bundles and vice versa.

An example of a lateral bundle sequence consisting of large-scale cross-bedded sets from the lower part of the Holocene succession of the Oosterschelde mouth is shown in Fig. 4 (see also VISSER, 1980 and SIEGENTHALER, 1982). These large-scale cross-bedded sets were produced by ebb-dominated currents. The lateral variation of bundle thicknesses is shown in Fig. 5, where the neap- and spring-tide periods are clearly differentiated. Each bundle was, according to VISSER (1980) and ALLEN (1981a), deposited during one single dominant tide. The complete preservation of the mud drapes allows one to assume that the erosion due to the subordinate flood current is small and that the original megaripple height can be reliably estimated from the set height (Fig. 3).

The presence of small ripples or megaripples would have a

Fig. 2 (facing page)
Stratigraphic scheme of the Holocene of the construction pit Schaar, showing the superposition of two tidal channel sequences. (modified after VAN DEN BERG, 1982). * Indicates the position of the measured bundle sequence (see Fig. 4).

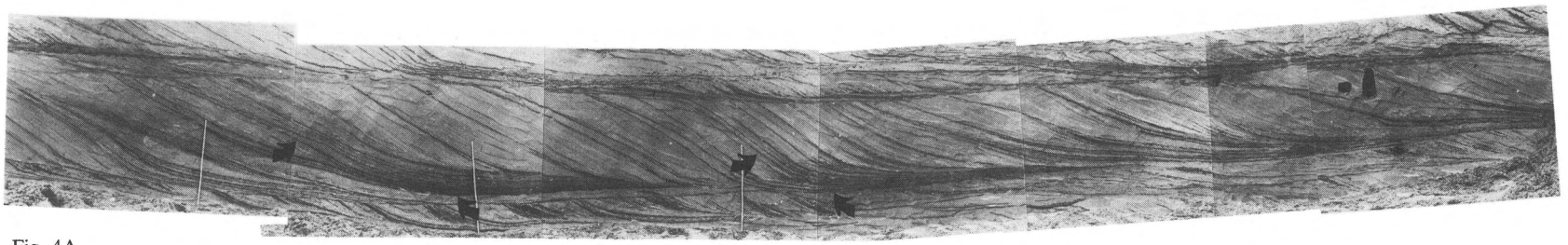

Fig. 4A
Photographic mosaic of part of the Holocene outcrop, showing an ebb-oriented set with a well developed lateral bundle sequence (base at approx. 15 m below MSL). Arrows indicate the position of the neap tide bundles.

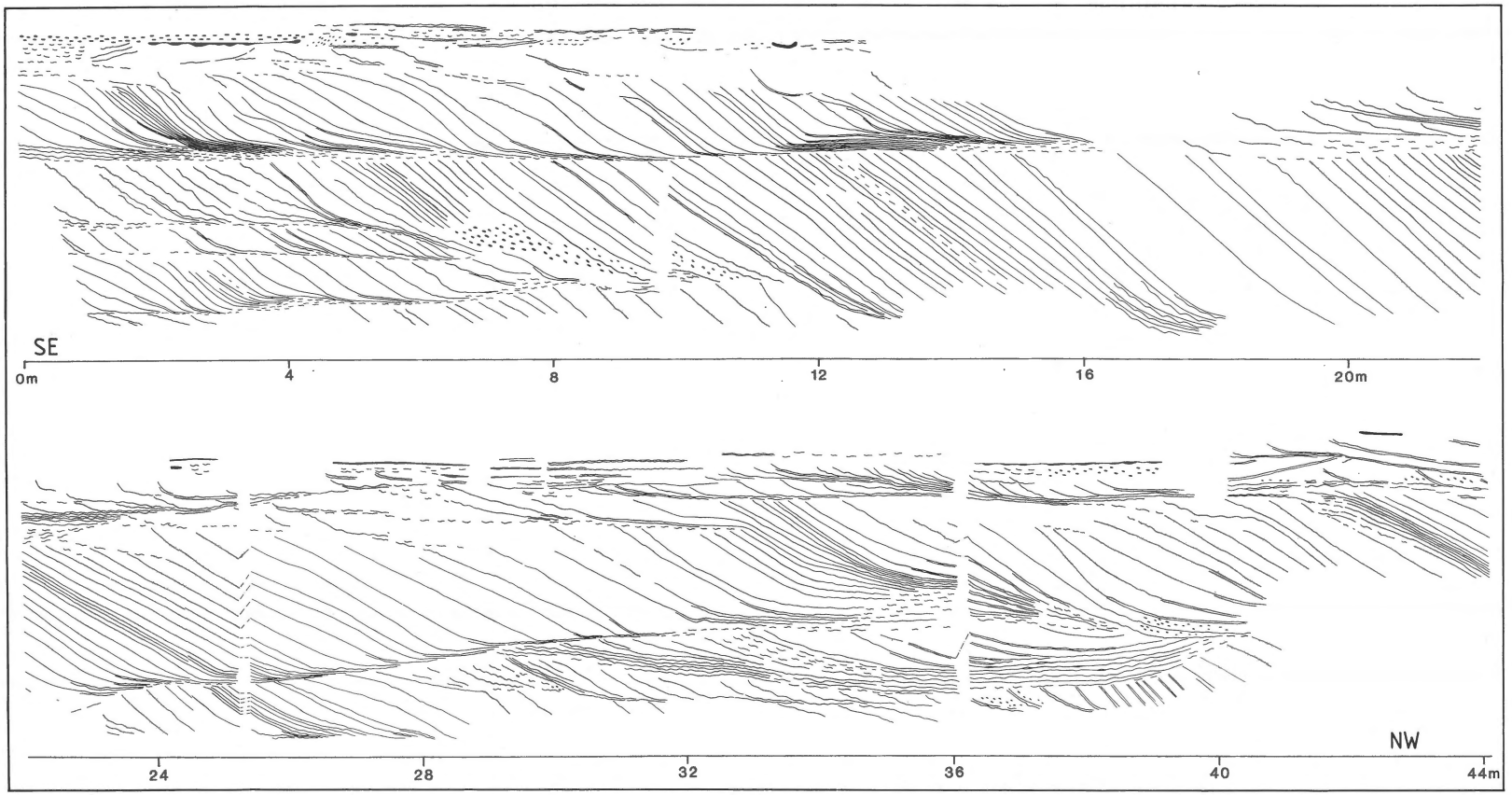

Fig. 4B
Drawing of a section through large ebb-oriented sets at 15-12 m below MSL. Only the mud drapes are drawn to show the bundle structure during neap and spring tide. Five neap-spring-neap tide periods are present in the main set; the random (aperiodical) bundle thickness variation is much greater at spring (thick bundles) than at neap. Field drawing by M. J. Visser (see also VISSER, 1980).

major effect on sediment movement. Following MIDDLETON & SOUTHARD (1978), we define bed-load as the sediment that is trapped in the lee of these bed forms (small ripples or megaripples), i.e. the sediment that contributes to the bed form migration. Therefore, the transport rates of the bed-load so defined are measured on the basis of the migration rates of these bedforms (BAGNOLD, 1941, KACHEL & STERNBERG, 1971, ALLEN, 1981b).

Based on the definition discussed above, the bundle thickness (f_i) and the megaripple height (h) represent the quantity of bed-load sediment transport (F_i) during a single dominant tide (i), trapped on the leeside of the megaripple. We can summarize this statement by:

$$F_i = h\, f_i\, \gamma'_g / \sin \beta \qquad \text{(eq. 1)}$$

assuming that the bundle thickness (f_i) is very small compared to the wavelength of the megaripple (TERWINDT, 1970).

There is a relationship between the bed-load sediment transport F_i and the hydraulic parameters such as the peak value of the shear velocity U_{*i} or the tidal range R_i.

The problem, however, is to establish the following variables and functions:

- the bed-load sediment transport function
- the magnitude of the shear velocities U_* during the tide i as a function of time t:

$$U_* = U_{*i}\, \phi\, (t) \qquad \text{(eq. 2)}$$

- the duration of the dominant tide. The period T of a complete ebb-flood tidal cycle is 12.4 hours in a semi-diurnal tidal system, which has about 28.5 ebb-flood tidal cycles per neap-spring-neap tidal period.
- a relation between the shear velocities and the tidal ranges based on an estimation of the water depth.

An important factor which influences the tidal processes is the atmospheric forces. The aperiodic or random variation component of the bundle thicknesses or the bed-load sediment transport (F) is caused by storms (Fig. 6). Storms affect both the duration and the strength of the tidal currents, expressed respectively by the parameters ϕ (t) and U_{*i}.

We will, however, only consider the changes of U_{*i}, which means that we will assume that the duration of the dominant tide is constant (= T/2). Because of the underestimation of the dominant tidal duration, this analysis will therefore slightly overestimate the atmospheric effects.

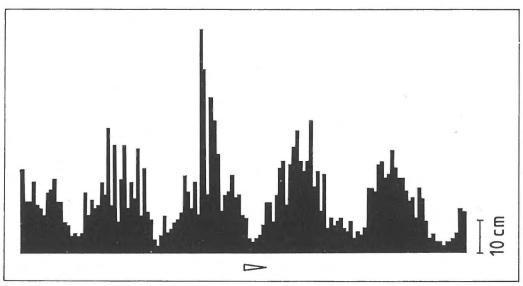

Fig. 5
Diagram showing the lateral thickness variation of the bundles of five neap-spring-neap tide cycles. Erosion due to the subordinate current is taken into account and the measurements represent an estimation of the bed-load sediment transport during dominant tidal cycles. The instantaneous thickness fluctuations are aperiodic and mainly due to storms (modified after VISSER, 1980).

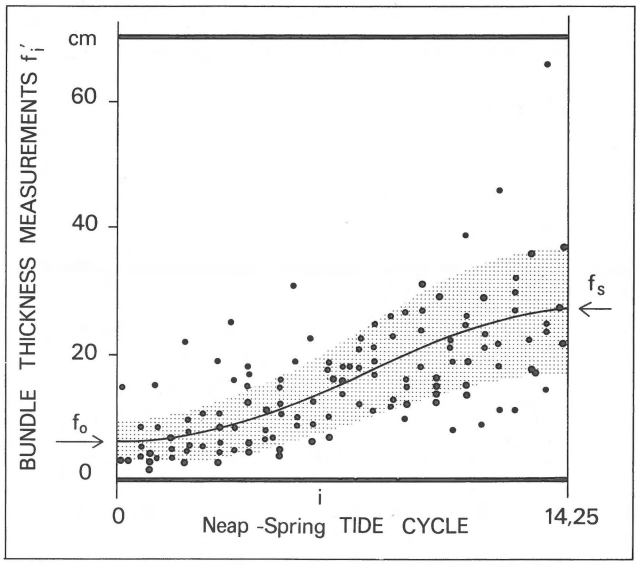

Fig. 6
Bundle thicknesses from Fig. 5 plotted in a single neap-spring cycle. The line gives the best fitting theoretical thickness distribution and the dotted area represents the theoretical thickness ± the standard deviation. The thicknesses at neap (f_o) and at spring (f_s) are resp. 6.3 cm and 26.7 cm.

SAMPLING AND EVALUATION OF FIELD DATA

A correct sampling of field data is essential for the calculation of the palaeotidal-hydraulics. The following data have to be collected in the field:

a. Establish a thickness sequence of the successive bundles. The thickness of a bundle is measured perpendicular to the boundaries of the bundle (e.g. the mud drapes) and the most suitable position is halfway between the top and the bottom of the preserved foreset (Fig. 3, see also VISSER, 1980).

Since the bundle thickness variations are used to estimate the variations of the sediment transport, it is necessary to eliminate the thickness variations due to irregular megaripple migrations, especially in the case of megaripples with an irregular sinuous crest pattern. Such megaripples show uneven levels of both crests and troughs, in contrast to the relatively straight crest and regular pattern of the so-called two-dimensional straight crested megaripples (HARMS ET AL., 1982). The cyclical character of the measured thicknesses should be obvious from a lateral bundle sequence

diagram (Fig. 5) or a thickness distribution diagram in neap-spring tidal cycles (Fig. 6). The cyclical character, if present, can also be proved by a Fourrier analysis (YANG & NIO, in press).

b. Estimate the original megaripple height from the height of the cross-bedding set (Fig. 3). This height should be corrected for a possible erosion after the deposition.
c. Measure the dip of the bundle foresets (Fig. 3).
d. Estimate the original water depth during the deposition of the measured beds.
e. Determine the grain size of the measured bundles.

THE SEPARATION OF A MEASURED BUNDLE-THICKNESS SEQUENCE INTO THE APERIODIC AND THE PERIODIC COMPONENTS OF A NEAP-SPRING TIDE CYCLE

For a normal semi-diurnal tidal system, the superposition of the sinusoidal lunar and solar components of the tides produces vertical tidal ranges R_i in the ebb-flood tidal cycle i. This is given by:

$$R_i = \{R_o^2/2+R_s^2/2+(R_o^2-R_s^2)\cos(\pi i/M1)/2\}^{1/2} \qquad \text{(eq. 3)}$$

where R_o and R_s are the tidal ranges at neap and at spring tide respectively. M1 is the number of tidal cycles from neap to spring tide.

From $f_i \propto R_i^n$ (see eq. 10, 11, 13, and II-5) and by using eq. 3, it follows that a periodic neap-spring tidal bundle thickness sequence of f_o, f_1 . . . f_s, produced by tidal currents alone, is given by:

$$f_i = \{f_o^{2/n}/2+f_s^{2/n}/2+(f_o^{2/n}-f_s^{2/n})\cos(\pi\, i/M1)/2\}^{n/2} \qquad \text{(eq. 4)}$$

where n is the exponent of the sediment transport function, f_o and f_s are the bundle thicknesses at neap and spring tide respectively, which are found by taking the least square fit of the calculated thicknesses f_i (eq. 4) in the measured thickness data set $f_1', \ldots, f_N'$. The least square fit is not sensitive on n. For n=2, a simple explicit solution for f_o and f_s is:

$$f_s/2-f_o/2 = (\Sigma f_j' \Sigma x_j - N\Sigma f_j' x_j)/[N\Sigma x_j^2-(\Sigma x_j)^2] \qquad \text{(eq. 5)}$$

$$f_s/2+f_o/2 = \{\Sigma f_j' + (f_s/2-f_o/2)\Sigma x_j\}/N \qquad \text{(eq. 6)}$$

$$x_j = \cos[\pi(j-M2)/M1]$$

$$j = 1, \ldots, N$$

where N is the number of the measured bundles. M2 is the position of the first neap tide and is found by Fourrier analysis (YANG & NIO, in press). The solution for the set of data in Fig. 5 is f_o = 6.3 cm and f_s = 26.7 cm (which are shown in Fig. 6 together with eq. 4); the correspondent M2 value is 12.35.

The expression for the mean bundle thickness is:

$$\bar{f} = \Sigma f_j/N \qquad \text{(eq. 7)}$$

The mean standard deviation of the aperiodical component is:

$$\overline{SD}\,(f) = \{\Sigma\,(f_j-\bar{f}_j)^2/(N-1)\}^{1/2} \qquad \text{(eq. 8)}$$

Calculations from the set of data in Fig. 5 show that $\bar{f}$ = 16.5 cm and $\overline{SD}$ (f) = 7.74 cm.

From $SD(f_i) \propto f_i$ (see eq. 19), we can deduce that the standard deviation of the bundle thicknesses increases from neap to spring tide:

$$SD\,(f_i) = f_i\,\overline{SD}\,(f)/\bar{f} \qquad \text{(eq. 9)}$$

THE CALCULATION OF PALAEOTIDAL FLOW VELOCITIES AND RANGES DURING MEAN, NEAP, AND SPRING TIDE

The flow chart in Fig. 7 shows schematically the relationship of the variables concerning the deposition of a tidal bundle sequence, as well as the steps for calculating the palaeotidal hydraulics. The definitions of the variables are given in notations (Appendix III). Some dimensionless variables (e.g. dimensionless sediment transport rate Φ, mobility number Y and its reciprocal Ψ) have the same meaning as widely used in hydraulic engineering (YALIN, 1972).

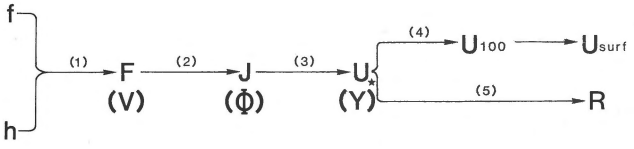

Fig. 7
Flow chart showing the relationship of variables concerning the tidal bundle sequence deposition. Numbers refer to the calculation steps.

Step 1: The determination of the bed load transport per unit width (F_i) during the dominant tide (i) and its dimensionless version (V_i).

If the erosion due to the subordinate current is small, the bundle thickness f_i and the megaripple height h define the bed-load sediment transport during a single dominant tide i (see eq. 1).

Its dimensionless version can be expressed in the following equations:

$$V_i = \frac{2\pi}{T}\int_o^{T/2} \Phi(t)dt$$

Notice the definitions of Φ (t) and F_i, we have:

$$V_i = \frac{2\pi}{T}\int_o^{T/2} gj(t)\, \rho^{1/2}/ (r_g D)^{3/2}\, dt$$

$$= \frac{2\pi g\, \rho^{1/2}}{T(r_g D)^{3/2}}\int_o^{T/2} j(t)\, dt$$

$$= \frac{2\pi g\, \rho^{1/2}}{T(r_g D)^{3/2}} F_i$$

From eq. 1, follows:

$$V_i = 2\pi\, f_i\, h\, \rho'_g\, g\, \rho^{1/2}/[T \sin \beta\, (r_g D)^{3/2}] \qquad \text{(eq. 10)}$$

where ß is the dip of the foresets. It is assumed that the megaripple has a triangular cross section and that f_i is very small as compared to the wavelength.

Step 2: The calculation of the peak value of the bed-load transport rate (J_i) during the dominant tide (i) and its dimensionless version Φ_i (for their derivation, see Appendix I):

$$\Phi_i = V_i / r \qquad \text{(eq. 11)}$$

$$J_i = \Phi_i\, (r_g D)^{3/2} / g \qquad \text{(eq. 12)}$$

where $r = \int_o^{\pi} \phi(x)\, dx$ and $\phi(x)$ describes the time dependent pattern of the tidal currents in an ebb-flood tidal cycle. The value of r is not very sensitive to the exact nature of the function ϕ (x) and is roughly $\pi/3$ for $n > 1.5$ (see Appendix I and Fig. 11 for details).

Step 3: The calculation of the peak value of the shear velocity (U_{*i}) during the dominant tide (i) and its dimensionless version (Y_i) using an appropriate bed-load transport function.

As already stated before, a crucial point here is the choice of an appropriate bed-load transport function. In this paper we use the empirically determined bed-load transport function as used in hydraulic engineering. Following the proposal of EINSTEIN (1942, 1950), YALIN (1972) plotted the bed-load transport rate data in a log graph (see Fig. 8). These data fit very well into the modified Einstein formula. On the other hand, KACHEL & STERNBERG (1971), based on their own data and experiments by GUY ET AL. (1966), predict a much lower transport rate, especially for small grain diameters. This difference is caused by the variation of the Reynolds number Re_*. YALIN's data were obtained mostly in rough flow conditions with a $Re_* > 70$, whereas the other data indicate much lower Re_* values (equivalent to transitional flow). Therefore an estimation of Re_* is necessary to interpret such a graph.

In our calculations we used the empirical bed-load transport rate formula of:

$$\Phi = a\Psi^{-n} \qquad \text{(eq. 13)}$$

which is a straight line in a log Φ-Ψ plot (see A, B, C in Fig. 8). The factor a and the exponent n are estimated graphically as explained in Appendix I. It is also shown that the error induced by the approximation of eq. 13 is unimportant. From this equation follows that:

$$Y_i = (\Phi_i/a)^{1/n} \qquad \text{(eq. 14)}$$

and

$$U_{*i} = (Y_i\, r_g\, D/\rho)^{1/2} \qquad \text{(eq. 15)}$$

The factor a and the exponent n of the bed-load sediment transport function are determined according to flow conditions. The values of a and n used in this study are:

- $a = 15.6 / n = 2.77$ (line C in Fig. 8) for the data from the Holocene subtidal deposits in the Oosterschelde;
- $a = 10.0 / n = 3.0$ (line A in Fig. 8) for a relatively low Re_*-value (KACHEL & STERNBERG, 1971) and
- $a = 12.3 / n = 1.71$ (line B in Fig. 8) for a relatively high Re_*-value ($Re_* > 70$; YALIN, 1972).

Step 4: The calculation of the peak value of the flow velocity at the surface ($U_{surf\ i}$) during the dominant tide (i), provided the water depth is known or can be estimated.

If the bottom friction is known, the flow velocity can be calculated from:

$$U_{100\ i} = U_{*i} / C_{100} \qquad \text{(eq. 16)}$$

where C_{100} is the friction coefficient at 1.00 m above the sediment interface and U_{100} is the corresponding flow velocity. A mean value for C_{100} is 0.0547 (STERNBERG, 1972).

If we assume that the boundary layer extends through the whole water column, then the velocity at the water surface can be calculated with the velocity defect law formula:

$$U_{surf\ i} = U_{100\ i}\, [1+2.5\, C_{100} \ln (H/100)] \qquad \text{(eq. 17)}$$

where H is the water depth (see YALIN, 1972; his eq. 2.78).

Step 5: The calculation of the tidal range (R_i), if the water depth (H) is known.

A suggestion for this calculation is given in Appendix II, where a connection between the peak value U_{*i} of the shear velocity in a tidal half cycle and the tidal range R_i is

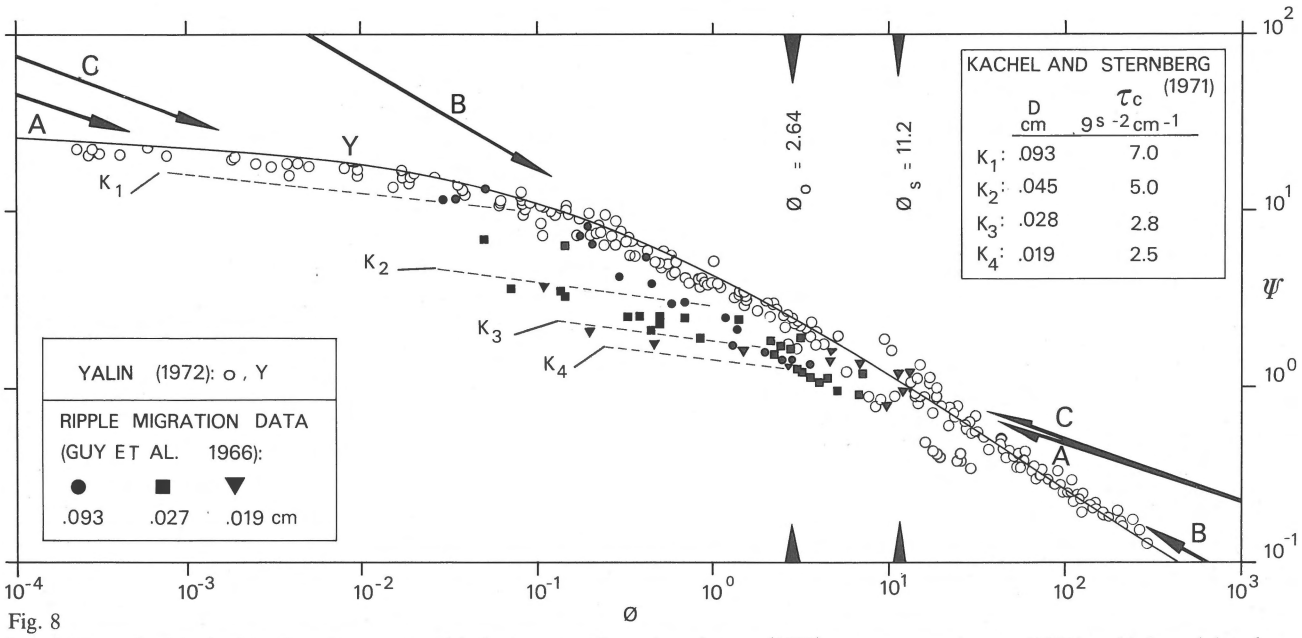

Fig. 8
Log Φ-Ψ graph of the bed-load transport rate, with the transport formulae of YALIN (1972), KACHEL & STERNBERG (1971) and inferred data from GUY ET AL. (1966). Φ_o and Φ_s are the peak values of the dimensionless transport rate calculated from the bundle thickness at neap and at spring tide (see Fig. 6). The straight lines A, B and C approximate the bed-load transport rate (see eq. 13).
A: calculation based on data from GUY ET AL. (1966) and KACHEL & STERNBERG (1971); B: calculation based on data from YALIN (1972); C: calculation based on data from present-day tidal parameters in the Oosterschelde (see also Table I).

established:

$$R_i = U_{*i}^2 T / [\pi(gH)^{\frac{1}{2}}] \qquad \text{(eq. 18)}$$

A tidal current pattern sin(t) is assumed for this equation. The use of this equation is tested in Fig. 9, where the magnitudes of especially the ebb currents are predicted rather well at location B. The values for the currents at location A, however, suggest a higher friction value, but are otherwise not conflicting. This equation can only be used for shallow water depths (not deeper than 30 m).

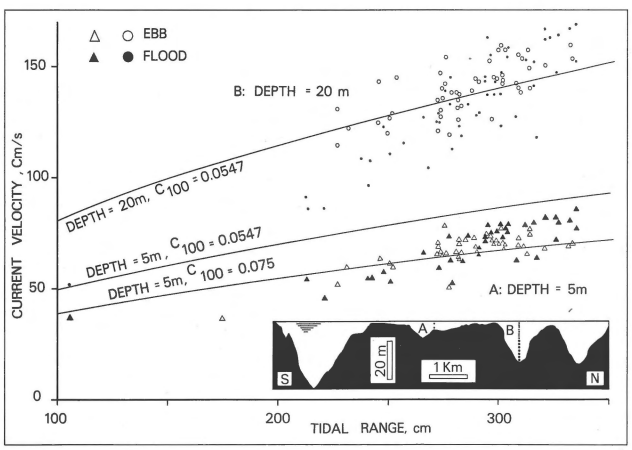

Fig. 9
Tidal ranges versus ebb and flood currents at two localities A and B, resp. 5 m and 20 m deep. The full lines are the theoretical solutions from eq. II-5. Inset shows a profile along the dam site with the locations A and B (Data from RIJKSWATERSTAAT, 1970).

THE ESTIMATION OF THE STORM STRENGTH FROM THE APERIODIC BUNDLE THICKNESS VARIATION

Assuming that the aperiodic bundle-thickness variation in the Holocene deposits of the Oosterschelde is mainly caused by current variations due to atmospheric forces (see Fig. 5 and Fig. 6), this variation can be used directly to estimate the storm strengths.

The aperiodic random thickness-variation component due to storms shows a tendency for a negative thickness auto-correlation of successive bundles; i.e. thick bundles tend to be compensated for by subsequent thin bundles and vice versa.

The storms affect both the duration and the strength of the tidal currents, expressed by the parameters ϕ (t) and U_{*i}, but only the changes of U_{*i} will be considered here.

Storms cause the water level to fluctuate around the tide-determined water level; these fluctuations are, however, independent of the absolute water level (see Fig. 10). The aperiodic component of the tidal range is, therefore, independent of the neap-spring tide cycle, i.e. $SD(R_i) = SD(R)$ and $SD(Y_i) = SD(Y)$.

According to the error propagation law:

$$SD(Y_i) = SD(f_i)\, \delta Y_i / \delta f_i \qquad \text{(eq. 19A)}$$

and using eq. 10, 11, 13, follows:

$$SD(Y) = (V_i/ar)^{1/n}\, SD(f_i)/(nf_i) \qquad \text{(eq. 19B)}$$

$$= (V_0+V_s)^{1/n}\, (2ar)^{-1/n}\overline{SD}(f)/(\bar{f}n) \qquad \text{(eq. 19C)}$$

where i = 1 or 2 or . . . . s, and $\bar{f}$ and $\overline{SD}(f)$ are the mean bundle thickness and the mean standard deviation defined in eq. 7 and 8. The exponent of the transport function n (see eq. 13) is larger than 1.5.

We can also write this in terms of the mean coefficient of variation:

$$\overline{VARC}(R) = \overline{SD}(R)/\bar{R} = \overline{SD}(f)/(\bar{f}n) = \overline{VARC}(f)/n \qquad \text{(eq. 20)}$$

We know that $SD(f_i)$ is a function of f_i. The values $f_i \pm SD(f_i)$ from the Holocene deposits of the Oosterschelde have been plotted in Fig. 6 assuming n = 2.77 (as in the case of f_i, $SD(f_i)$ is not sensitive to the value of n). Approximately 75% of all the data are scattered regularly from neap to spring tide within the plotted area. This is a strong indication that parameters other than the tidal range (e.g. the ripple geometry, the duration of the dominant tidal cycle or the function ϕ (t)) do not contribute substantially to the aperiodic bundle thickness variation. This also means that r = constant and $F_i \propto f_i$).

We can in a similar way calculate the statistic parameters of the shear velocity and eventually of the flow velocity.

CONCLUSIONS

A summary of the results is presented in Table I. Three solutions are presented here (compare also with Fig. 8):

A: with relatively low Re_*, equivalent to smooth and transitional flow (GUY ET AL., 1966; KACHEL & STERNBERG, 1971);

B: with relatively high Re_* (YALIN, 1972) and

C: adapted Re_* values for the present-day Oosterschelde tidal basin.

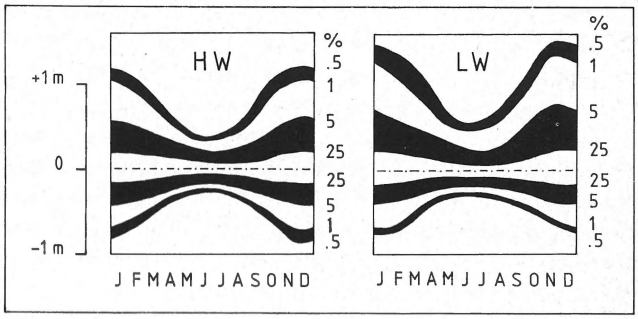

Fig. 10
Diagram showing the probability of aperiodic water level deviations at high water (HW) and at low water (LW) at Vlissingen (Data from RIJKSWATERSTAAT, 1979). J, F, ..., D refer to the months of January, February, ..., December.

The standard deviations SD(R) in C can roughly be compared with the standard deviation of the predicted sea level during winter at Vlissingen (see Fig. 10). Storms in this area are of relatively short duration, mostly less than one tidal cycle. It is therefore reasonable to assume that the aperiodic standard deviation of the water level at low or high water should roughly correspond to the aperiodic standard deviation of the tidal range.

In above analysis, a correct identification of subtidal megaripple cross-bedding with lateral bundle sequence and the genetic interpretation of these tidal structures, as well as a careful sampling of field data are essential to further evaluation. Based on these conditions, a series of important functions, which relate tidal processes with their preserved products, can be used to characterize in a quantitative way the hydraulics of the palaeo-environment. Two different levels of approach are proposed:

- A simple relation connects the mean coefficient of the aperiodic variation of the bundle thickness with the mean coefficient of the aperiodic variation of the tidal range caused by atmospheric processes, such as storms.
- A careful application of the bed-load sediment transport rate relations leads to the mean-, neap-, or spring-tide shear velocities and also to the corresponding tidal ranges.

Table I
Summary of the hydraulic parameters reconstructed from the bundle thicknesses in Fig. 5. The solutions A, B and C refer to the transport rate shown in Fig. 8.

parameters		n	a	Y_i	u_{*i} cm/s	Re_{*i}	u_{surfi} cm/s	R_i cm	SD(Y)	SD(R) cm	$\overline{VARC}(R)$ %
A	neap	3.0	10.0	.64	4.6	9.2	114	252	.14	54	16
	spring			1.04	5.8	11.6	145	407			
B	neap	1.71	12.3	.41	3.6	7.2	91	160	.20	77	27
	spring			.95	5.5	11.0	139	371			
C	neap	2.77	15.6	.53	4.1	8.2	103	206	.13	49	17
	spring			.89	5.4	10.8	134	347			

The present reconstruction is an attempt to interpret quantitatively sedimentary features with the current knowledge of the tidal hydraulics and of the sediment transport. The applicability has been demonstrated to Holocene subtidal deposits of the Oosterschelde mouth (200-300 years old). Since the periods of the tides have hardly changed during Phanerozoic time (SCRUTON, 1978), the application of this method to older subtidal deposits is possible if a genetic interpretation for tidal deposits and the recognition of a lateral bundle sequence is well established.

ACKNOWLEDGEMENTS

The authors want to thank all the members of the Comparative Sedimentology Division for their help in the field and their discussions and criticism. Special thanks are due to the members of Rijkswaterstaat/Deltadienst in Zierikzee and Den Haag for their support and supply of data. We are also grateful for the discussions and suggestions of Thomas Teyssen, University of Bonn, Germany.

REFERENCES

Allen, J. R. L. 1981a Lower Cretaceous tides revealed by cross-bedding with mud drapes – Nature 289: 579-581.

—— 1981b Paleotidal speeds and ranges estimated from cross-bedding sets with mud drapes – Nature 293: 394-396.

Allen, P. A. & P. Homewood (in press) Evolution and mechanics of a Miocene tidal sandwave.

Bagnold, R. A. 1941 The physics of blown sand and desert dunes – Morrow (New York): 265 pp.

Boersma, J. R. 1967 Remarkable types of mega cross-stratification in the fluviatile sequence of a subrecent distributary of the Rhine – Geol. Mijnbouw 46: 217-235.

—— 1969 Internal structures of some tidal mega-ripples on a shoal in the Westerschelde estuary, The Netherlands – Geol. Mijnbouw 48: 409-414.

Einstein, H. A. 1942 Formulae for the transportation of bed load – Trans. A.S.C.E. 107.

—— 1950 The bed-load function for sediment transportation in open channel flows – U.S. Dept. Agriculture, Soil Conservation Ser., Tech. Bull. 1026.

Guy, H. R., D. B. Simons & E. V. Richardson 1966 Summary of alluvial channel data from flume experiments, 1956-1961 – U.S. Geol. Survey Prof. Paper 462-I (Washington).

Harms, J. C., J. B. Southard & R. G. Walker 1982 Structures and sequences in clastic rocks – S.E.P.M. Short Course 9, Calgary: 2.1-2.55.

Kachel, N. B. & R. W. Sternberg 1971 Transport of bedload as ripples during an ebb current – Mar. Geol. 10: 229-244.

Langhorne, D. N. 1981 An evaluation of Bagnold's dimensionless coefficient of proportionality using measurements of sandwave movement – Mar. geol. 43: 49-64.

Middleton, G. V. & J. B. Southard 1978 Mechanics of sediment movement – S.E.P.M. Short Course 3, Binghamton (New York): 6.29-6.50.

Scruton, C. T. 1978 Periodic growth features in fossil organisms and the length of the day and the month. In: P. Brosche & J. Sundermann (eds): Tidal friction and the Earth's rotation – Springer Verlag (New York): 154-196.

Siegenthaler, C. 1982 Tidal cross-strata and the sediment transport rate problem: a geologist's approach – Mar. Geol. 45: 227-240.

Sternberg, R. W. 1972 Predicting initial motion and bedload transport of sediment particles in the shallow marine environment. In: D. J. P. Swift, D. B. Duane & O. H. Pilkey (eds) Shelf sediment transport: process and pattern – Dowden, Hutchinson and Ross (Stroudsburg): 61-82.

Terwindt, J. H. J. 1970 Observation on submerged sand ripples with heights ranging from 30 to 200 cm occurring in tidal channels of S. W. Netherlands – Geol. Mijnbouw 49: 489-501.

Teyssen, T. (in press) Physical model and FORTRAN IV program to estimate paleotidal flow velocities from features of sand waves.

Van den Berg, J. H. 1981 Rhythmic seasonal layering in a mesotidal channel fill sequence, Oosterschelde mouth, the Netherlands. In: S. D. Nio, R. T. E. Schuttenhelm & Tj. C. E. van Weering (eds): Holocene marine sedimentation in the North Sea basin – IAS Spec. Publ. 5, Blackwell (Oxford): 147-159.

—— 1982 Migration of large-scale bedforms and preservation of crossbedded sets in highly accretional parts of tidal channels in the Oosterschelde, SW Netherlands – Geol. Mijnbouw 61: 253-263.

Visser, M. J. 1980 Neap-spring cycles reflected in Holocene subtidal large-scale bedform deposits: a preliminary note – Geology 8: 543-546.

Visser, M. J. & P. L. de Boer (in press) The diurnal inequality of the tide as a tool in the recognition of tidal deposits.

Rijkswaterstaat 1970 report 17.4 & 14.5

Rijkswaterstaat 1979 Getijtafels voor de Zeehavens in Nederland en voor Antwerpen.

Yalin, M. S. 1972 Mechanics of sediment transport – Pergamon Press (Oxford): 292 pp.

Yang, C. S. & S. D. Nio (in press) The estimation of paleohydrodynamic processes from subtidal deposits using time series analysis methods.

APPENDIX I: THE TIME-DEPENDENT PATTERN OF TIDAL CURRENT VELOCITIES AND THE CALCULATION OF ITS INTEGRATION

The magnitudes of the shear velocities U_* during the tide i changes as a function of time t:

$$U_* = U_{*i}\,\phi(t) \qquad \text{(I-1)}$$

where U_{*i} is the peak shear velocity of tide i, and $\phi(t)$ describes the time depentent pattern of the tidal currents in tide i. This pattern is quite similar at a neap and at a spring tide cycle for a given location (SIEGENTHALER, 1982). Therefore, the function $\phi(t)$ is the same throughout the spring-neap tide cycle:

$$\phi_o(t) = \phi_s(t) = \phi_i(t) = \phi(t) \qquad \text{(I-2)}$$

$\phi(t)$ is unknown if fossil cross-beds are analysed; the most 'natural' expression is $\phi(t) = \sin(t)$. It is shown later that in most cases the form of the function $\phi(t)$ does not greatly influence the result.

If eq. 13 is used as a bed-load transport function, then:

$$V_i = 2\pi/T \int_o^{T/2} \Phi(t)dt$$

$$= 2\pi/T \int_o^{T/2} aY^n(t)dt$$

From eq. I-1, I-2, and notice the definition of Y_i, follows:

$$V_i = 2\pi/T \int_o^{T/2} a \int^n U_i^{2n}\phi^{2n}(t)(r_g D)^{-n}dt$$

$$= a[\int^n U_i^2(r_g D)^{-1}]^n\, 2\pi/T \int_o^{T/2} \phi^{2n}(t)dt$$

$$= aY_i^n\, r$$

$$= \Phi_i\, r \qquad \text{(I-3)}$$

$$\Phi_i = V_i / r \qquad \text{(I-4)}$$

$$\text{with } r = \int_o^{\pi} \phi^{2n}(x)dx \qquad \text{(I-5)}$$

$$Y_i = \int U_i^2 /(r_g D) \qquad \text{(I-6)}$$

Φ_i is the peak value of the dimensionless transport rate in the dominant cycle i and is a simple function of V_i and r. The value of r for different functions of $\phi(t)$ is given in Fig. 11.

Two important conclusions can be drawn:

1. The value of r is not very sensitive to the exact nature of the function $\phi(t)$ and is roughly $\pi/3$ for $n > 1.5$, if type II and type III are discarded as being unrealistic.
2. The most important contribution to the total bed-load transport during a dominant cycle occurs around the peak value of the shear velocity (compare type I with type V). Therefore a transport formula represented by a straight line in a log Φ-Ψ plot and intersecting the graph of the 'true' bed-load transport function at Φ_0 and at Φ_s will produce approximately the same bundle thickness as the 'true' bedload transport formula itself. Giving consideration to a possible effect of the Reynolds number Re_*, the factor a and the exponent n of eq. 13 can then be determined graphically from such a plot as Fig. 8. Using this empirical bed-load transport function, Y_o and Y_s (and therefore also the correspondent shear velocities, U_{*o} and U_{*s}) can be evaluated.

As a general rule this technique will slightly underestimate the mobility number Y_o at neap and overestimate Y_s at spring tide. This is because the Reynolds number (Re_*) is lower than average in neap tide and higher than average in spring tide. The bundles of the Oosterschelde example have the mean thicknesses of $f_o = 6.3$ cm at neap and $f_s = 26.7$ cm at spring tide (see Fig. 6) and the dimensionless bed-load transport rates are $\Phi_o = 2.64$ and $\Phi_s = 11.2$. Three solutions for eq. 13 are shown in Fig. 8 and given in Table I together with the resulting hydraulic parameters.

APPENDIX II: THE RELATION BETWEEN THE MOBILITY NUMBER AND THE TIDAL RANGE

In the whole Oosterschelde basin the empirical relationship

$$Ui \propto Ri^{1/2} \qquad \text{(II-1)}$$

(SIEGENTHALER, 1982) is found to exist independently of the water depth. This fact suggests the following reasoning. If the tides are considered to be a wave with wave length

$$\lambda = T(gh)^{1/2} \qquad \text{(II-2)}$$

the maximum tilt of the water surface will be

$$S_i = \pi R_i/\lambda = \pi R_i (gh)^{-1/2}/T \qquad \text{(II-3)}$$

time–velocity pattern	I 	II 	III 	IV 	V 
$\phi(x)$	$\sin(x)$	1	$\begin{pmatrix} 2x/\pi \\ 2-2x/\pi \end{pmatrix}$	$\begin{pmatrix} 1.5x/\pi \\ 1 \\ 1.5-\ 1.5x/\pi \end{pmatrix}$	$\begin{pmatrix} 0 \\ 1 \end{pmatrix}$
$r = \int_o^{\pi} \phi^{2n}(x)dx$	$\pi\,\frac{\Gamma(n+.5)}{2\Gamma(n+1)}$	π	$\frac{\pi}{2n+1}$	$\frac{\pi}{3}\left(1+\frac{2^{1-2n}}{2n-1}\right)$	$\frac{\pi}{3}$

Fig. 11
The value of $r = \int_o^{\pi} \phi^{2n}(x)dx$ for different current patterns during a single dominant tidal cycle.

Eq. II-3 is an expression for a progressive wave and is strictly valid only around the nodes in the case of a standing wave. Since $U_{\hat{i}}^2 = g\,hS_i$, the tidal range R_i is:

$$R_i = U_{\hat{i}}^2 T(gh)^{-1/2}/\pi \qquad \text{(II-4)}$$

and the peak value of the mobility number is

$$Y_i = \pi R_i \rho (gh)^{1/2}/(TDr_g) \qquad \text{(II-5)}$$

APPENDIX III: NOTATIONS

a	factor in the bed-load transport rate formula
c_{100}	friction coefficient, 0.0547
D	grain size, (cm)
f	bundle thickness, measured perpendicular to the foreset plane (cm)
F	bed-load transport per unit width during one dominant tide (g/cm)
g	acceleration due to gravity (981 cm/s^2)
h	megaripple height (cm)
H	water depth (cm)
J	bed-load sediment transport rate (g/cm s)
M1	number of tidal cycles from neap to spring tide (14.25)
M2	position of the first neap tide
n	exponent in the bed-load transport rate formula
N	number of the measured bundles (131)
r	$= \int_o^{\pi} \phi(x)dx$, $\pi/3$
R	tidal vertical range (cm)
Re_*	$= U_* D/\upsilon$, Reynolds number
S	slope of the water level
SD(x)	standard deviation of x
T	period of the tidal cycle (12.4×3600 s)
U	flow velocity (cm/s)
U_{surf}	flow velocity at the surface (cm/s)
U_{100}	flow velocity 100 cm above the bed (cm/s)
U_*	$= (\tau/p)^{1/2}$, shear velocity (cm/s)
V	= 2Fg/[T(r D)], dimensionless version of F
VARC(x)	= SD(x)/$\bar{x}$, coefficient of variation of x
Y	$= \rho U_{\hat{i}}^2/(r_g D)$, mobility number, a dimensionless version of shear velocity.
β	dip of the foreset plane, 30^0
r_g	$= g\,(\rho_g - \rho)$, submerged specific weight of the grain (981×1.65 g/s^2 cm^2)
λ	wave length of the tidal wave (cm)
ρ	density of the water (1 g/cm^3)
ρ_g	density of the grain (2.65 g/cm^3)
ρ_g'	bulk density of the sediment (1.6 g/cm^3)
φ(t)	function describing the tidal current pattern in a tidal cycle
Φ	$= g\,j\,\rho^{1/2}/(r_g D)^{3/2}$, dimensionless bed-load transport rate
Ψ	$= Y^{-1}$

The subscript i designates the peak value of a parameter in the tidal cycle i, where i = o is neap tide and i = s is spring tide. Φ_i, Φ_o and Φ_s are the peak values of the transport rate Φ in the tidal cycle i, at neap and at spring respectively; f_i and F_i refer to f and F in the cycle i. A bar ($\bar{}$) designates a mean value.